Zhang *et al. Microstructures* **2025**, *5*, 2025069
DOI: 10.20517/microstructures.2024.173

Microstructures

Research Article

Open Access

Atomic structure of the phase interface in hafnium oxide-based thin films

Sirui Zhang[1], Xinpeng Mu[2], Qijun Yang[1], Borui Wang[1], Jiajia Liao[1,3], Yichun Zhou[1], Qiong Yang[2], Min Liao[1]

[1]School of Advanced Materials and Nanotechnology, Xidian University, Xi'an 710126, Shaanxi, China.
[2]Key Laboratory of Low Dimensional Materials and Application Technology of Ministry of Education, School of Materials Science and Engineering, Xiangtan University, Xiangtan 411105, Hunan, China.
[3]Guangzhou Institute of Technology, Xidian University, Guangzhou 510555, Guangdong, China.

Correspondence to: Prof. Qiong Yang, School of Materials Science and Engineering, Xiangtan University, Yuhu District, Xiangtan 411105, China. E-mail: qyang@xtu.edu.cn; Prof. Min Liao, School of Advanced Materials and Nanotechnology, Xidian University, 266 Xinglong Section of Xifeng Road, Xi'an 710126, Shaanxi, China. E-mail: mliao@xidian.edu.cn

How to cite this article: Zhang, S.; Mu, X.; Yang, Q.; Wang, B.; Liao, J.; Zhou, Y.; Yang, Q.; Liao, M. Atomic structure of the phase interface in hafnium oxide-based thin films. *Microstructures* **2025**, *5*, 2025069. https://dx.doi.org/10.20517/microstructures.2024.173

Received: 24 Dec 2024 **First Decision:** 5 Feb 2025 **Revised:** 17 Feb 2025 **Accepted:** 28 Feb 2025 **Published:** 13 Jun 2025

Academic Editors: Zhihua Sun, Haijun Wu **Copy Editor:** Xing-Yue Zhang **Production Editor:** Xing-Yue Zhang

Abstract

Significant progress has been made in studying the microscopic mechanism of ferroelectricity in HfO_2 thin films. However, there is still insufficient research on the atomic arrangement and underlying principles of domain and phase boundaries. The atomic structure near the interface boundary can provide insights into the formation principles of phase boundaries, enabling a better understanding of phase stability, domain switching, and phase transformation. In this study, the aberration-corrected scanning transmission electron microscope is used to investigate the atomic structure of HfO_2 materials at the boundaries. The study reveals the formation of orthorhombic phase (O phase)/monoclinic phase (M phase) interfaces throughout the entire grain, with both coherent interface and incoherent interfaces. By examining the atomic structure at these boundaries, we explain the strain and the structure of atoms at different phase boundaries. In a coherent interface, 90° charged domain walls and 90° uncharged domain walls are found, where charged domain walls have positively charged (oxygen-ion diminishing) and negatively charged (oxygen-ion accumulating) interfaces due to the polarization change in the direction perpendicular to the domain walls. In addition, the O phase/M phase coherent interface possesses a transition region between the O phase and M phase, but there is a stepped phase boundary structure in the O phase/M phase incoherent interface due to the high mismatch stress. These studies provide favorable assistance for the microstructure of phase stability and the evolution laws of phase transitions.

Keywords: HfO_2 film, ferroelectric, interface structure, aberration-corrected scanning transmission electron microscope

INTRODUCTION

Ferroelectric materials exhibit unique ferroelectric properties characterized by stable ordered electrical dipoles, and their polarization can be reversed by applying an applied electric field[1-3]. These materials are well-suited for applications in non-volatile memory, including ferroelectric random-access memory (FeRAM), ferroelectric field-effect transistor (FeFET), *etc.*[4-6]. However, traditional ferroelectric materials like perovskites tend to lose their ferroelectricity as they get smaller in size due to the size effect[7,8]. This limitation prevents their effective integration with advanced semiconductor processes. In 2011, Böscke *et al.*[9] reported that Si-doped HfO_2 thin films displayed ferroelectric properties, which could be maintained even at thickness below 1 nm[10,11]. This discovery has sparked significant interest in HfO_2-based ferroelectric thin films and their potential applications, particularly in the field of electronic information technology[12-14]. The atomic structure of these films plays a crucial role in understanding their properties[15,16]. Microstructure studies of HfO_2-based ferroelectric thin films have revealed the existence of multiple different phase structures within HfO_2[17,18], including room temperature monoclinic phase (M phase, space group: $P2_1/c$), high-temperature tetragonal phase (T phase, space group: $P4_2/nmc$) and cubic phase (C phase, space group: $Fm3m$). It is important to note that all of these phases are centrosymmetric and non-polar. It was reported that the ferroelectricity in HfO_2-based thin films originates from a non-centrosymmetric orthogonal phase (O phase, space group: $Pca2_1$) in 2011[9], as evidenced in 2015[19] by scanning transmission electron microscopy (STEM) and position averaged convergent beam electron diffraction (PACBED)[20] methods. Researchers have also found that ferroelectric orthorhombic phases can be stabilized by doping different elements and adjusting the concentration of oxygen vacancies[21,22]. However, it should be noted that HfO_2-based thin films are typically polycrystalline due to the traditional growth process and other factors[23,24]. In other words, HfO_2-based thin films naturally possess a polycrystalline and multiphase structure.

Under various external conditions, such as an electric field[25], temperature[26], strain from different sources[27], *etc.*, transitions between different phases can occur[28,29]. The non-centrosymmetric ferroelectric O phase in $Hf_{0.5}Zr_{0.5}O_2$ (HZO) thin films is a metastable state, making it a popular research topic to investigate how other phases can transform into the O phase[30,31]. Recent studies using the aberration-corrected scanning transmission electron microscope (*Cs*-STEM) have shown that under the action of an external electric field, a transition between the polar $Pbc2_1$ phase and the non-polar $Pbca$ phases can occur[32], resulting in a change in the ferroelectric property of HfO_2. Additionally, fatigued thin films can regain their vigor by applying slightly higher voltages, indicating that these transitions are reversible. During the phase transformation process, there is also evidence of multiphase coexistence[33], making the phase boundary between different phases particularly important[34]. Therefore, understanding the microstructure of phase interfaces at the atomic scale is crucial for gaining a deeper understanding of HfO_2 thin films.

In this study, we fabricate a TiN/HZO/TiN film system. It is found that there is a multiphase coexisting structure within the film system in the entire grain. By utilizing *C*s-STEM, we find the coexistence of the O phase and M phase. Further analysis of the interface structure within the thin film unveils different atomic structures in coherent and incoherent interfaces. The coherent interface displays a transition layer in the O/M multiphase coexisting structure. There are two connected 90° domain structures, one of which exhibits band bending due to the charged domain walls. On the other hand, the incoherent interface exhibits a stepped structure, which is attributed to the high strain energy present in this region.

MATERIALS AND METHODS

The 50-nm-thick TiN bottom electrode was grown on a cleaned and heavily doped p-type silicon wafer using magnetron sputtering. By alternating deposition of HfO_2 and ZrO_2 layers (HfO_2 and ZrO_2 cycle ratio of 1:1) through atomic layer deposition (ALD) process, HZO ferroelectric thin film with a thickness of

approximately 15 nm was formed. The precursors used for the deposition process were $[(CH_3)_2N]_4Hf$ (TDMAHf) for Hf, $[(CH_3)_2N]_4Zr$ (TDMAZr) for Zr, and H_2O for O, respectively. To achieve post-metallization annealing (PMA), a TiN top electrode with a thickness of 50 nm was subsequently deposited at room temperature using magnetron sputtering. Finally, a rapid thermal annealing (RTA) process was conducted at 450 °C for 30 s in a N_2 environment to induce crystallization. For the STEM experiments, cross-sectional TEM samples were prepared by slicing, gluing, grinding, and dimpling. The final ion milling was performed using a Gatan PIPS system. The high-angle-annular-dark-field scanning transmission electron microscopy (HAADF-STEM) images were acquired using the JEOL ARM 200 kV microscope.

The density functional theory (DFT) calculations were performed using the projector augmented wave (PAW) method as implemented in the Vienna Ab initio Simulation Package (VASP). Perdew-Burke-Ernzerhof (PBE) generalized gradient approximation functional was used to deal with the exchange-correlation effects. The 9 × 9 × 9 and 7 × 1 × 7 Monkhorst-Pack k-point meshes were used for the HfO_2 unit cell and DW structure calculations, respectively. The plane wave truncation energy was set to 500 eV. The lattice and atomic positions were both fully relaxed until the Hellmann-Feynman force on each atom was less than 0.01 eV/Å.

RESULTS AND DISCUSSION

Coherent interface

The microstructure of the TiN/HZO/TiN system was analyzed using HAADF-STEM, as depicted in Figure 1A. Through thickness measurements, it was determined that the HZO film has a thickness of approximately 15 nm. The overall thickness of the HZO film is relatively uniform, but it exhibits some fluctuations, likely due to the presence of polycrystallinity. The TiN bottom electrode displays a columnar crystal structure, which can be attributed to the growth process involving magnetron sputtering. However, in Figure 1A, the top electrode is not visible as it was subtracted by the ion beam during the TEM sample preparation.

To examine the microstructure of HZO films in detail, high-resolution HAADF-STEM observations were conducted on a large grain within the films, leading to the findings depicted in Figure 1B. According to the introduction, multiple phases (O phase, M phase and T phase) coexist in the HZO film. The black arrows in Figure 1B indicate distinct boundaries, which arise from noticeable lattice changes within the film. By analyzing the arrangement of Hf/Zr atoms, different atomic arrangement regions can be easily distinguished. Thus, the presence of two visually distinct regions separated by black arrows is identified in Figure 1B. Furthermore, the intermediate region indicated by the red arrow exhibits distinct characteristics compared to the two neighboring regions.

Figure 1B was further analyzed using the geometric phase analysis (GPA), which relies on geometric operations to determine the relative magnitude of microstrain from high-resolution TEM images[35]. The corresponding strain image obtained from GPA is shown in Figure 1C. By examining the different strains, it becomes easier to identify the different structures through different colors, which are also separated by the black arrows. Figure 1D is obtained by profiling the blue line from Figure 1C, and the black arrow also indicates the boundary of the different regions, while the red arrow indicates the width of this phase boundary. As can be observed from Figure 1B, the strain in the left, middle and right regions exhibits a gradual increase. The strain in the middle region is intermediate between those in the two other regions, indicating that the lattice parameters in the middle region are distinct from those in the two regions depicted in Figure 1B.

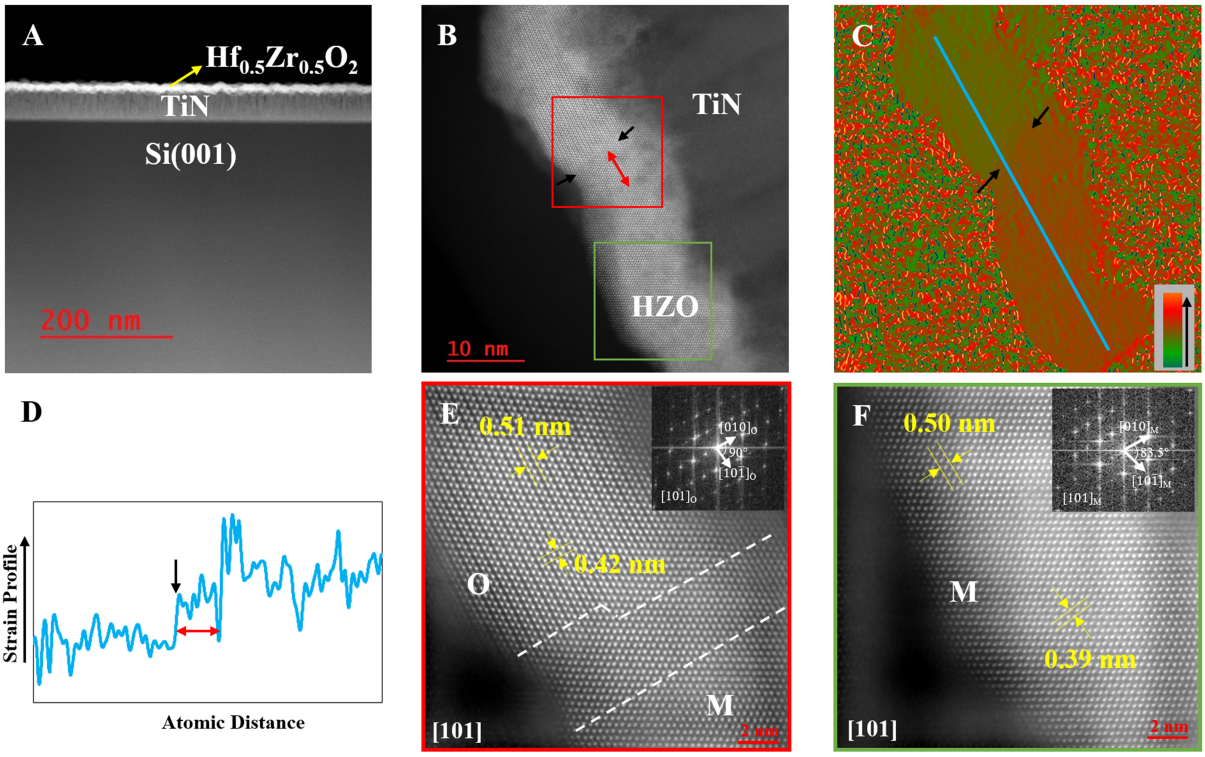

Figure 1. (A) Low magnification morphology image of grown TiN/HZO/TiN thin films; (B) The TiN/HZO/TiN thin film in a grain; (C) GPA performed in (B); (D) The strain profile corresponding to the blue line in (C). The black arrows represent the interface; the red arrows indicate the transition region; (E) High-resolution image of the upper half of the grain in (A); (F) High-resolution image of the lower half of the grain in (A). The area indicated by the white dashed line is the transition layer. HZO: $Hf_{0.5}Zr_{0.5}O_2$; GPA: geometric phase analysis.

To analyze the coexistence of the two-phase structure at the atomic scale in Figure 1B, high magnification atomic-scale HAADF-STEM imaging was conducted on the polyphase region, as shown in Figure 1E and F. Figure 1E represents the high-magnification image of the red box in Figure 1B, while Figure 1F corresponds to the green box in Figure 1B. According to literature reports, the atomic spacing between Hf/Zr atoms in the O phase exhibits a periodic pattern of one long and one short, while the characteristic angle of the M phase is not 90°. It is obvious that there are two types of phase structures in Figure 1E and F, because the Hf/Zr atoms in Figure 1E have one long and one short periodicity. In Figure 1E, the fast Fourier transform (FFT) operation, which is inset, was performed on the region inside the red box to obtain its electron diffraction pattern inset. By analyzing the electron diffraction pattern and comparing it with the PDF standard card, the interplanar spacing value and angle were measured. This analysis confirmed that the region corresponds to the O phase in the [110] direction. Similarly, in Figure 1F, the same analysis was performed on the region inside the green box, resulting in the obtained FFT inset. This analysis further confirmed the presence of the M phase of HZO with orientation along [110]. Therefore, based on these observations, it can be concluded that there is a coexistence of the M phase and the O phase in Figure 1B.

It can be observed that the region demarcated by the white dotted line in Figure 1E corresponds to the area indicated by the red arrow in Figure 1B. The lattice arrangement reveals inconsistencies with both the O phase and the M phase. Hence, the phase structure of this region cannot be determined. However, considering the results of the GPA analysis [Figure 1C], it is believed that this region is a transition region, bridging the O phase and the M phase. Consequently, the strain in this region lies between the two phases. This finding is consistent with the area represented by the red arrow in Figure 1D. Upon analyzing the

interface indicated by the white dashed line between the O phase and the transition region, it is apparent that it is not flat, while the lank interface between the transition region and the M phase appears relatively flat. And the irregularity interface may be caused by the spontaneously polarized charge in the O phase, which lead to the aggregation of oxygen vacancies.

As shown in Figure 2, another coherent interface appears in the HZO film. Figure 2A shows the intact crystal particle in the HZO film, and it is clear from the HAADF-STEM image that there is only one phase structure in the grain, except for the part in the red box in the upper left corner. Therefore, the area in the red box was enlarged and rotated 90° to obtain Figure 2B, which is also convenient for subsequent research. Several interfaces were analyzed using atomic models and other methods, as shown by the white dashed line in Figure 2B. The atomic model structure was used to illustrate the interface structure in Figure 2B, as shown in Figure 2C. The structure includes two types of interfaces, namely $O_{[010]}/O_{[001]}$ and $O_{[001]}/O_{[010]}$ interfaces, which are drawn with blue dashed lines. The difference between this interface and the interface in Figure 1 is that both sides of the interface belong to the O phase structure, so the interface structures in Figure 2B are the domain structure. The difference is that the polarization directions in the three parts are different. In order to study the stability of the structure, the DFT calculation is used to simulate the observed two neighboring 90° domain walls (DWs) of HfO_2. The top panel of Figure 2C sketches the 90° DW structure, which involves three domain regions and two DWs. The atomic and electronic structures of the two types of DWs are calculated within a 1 × 8 × 1 supercell as in our previous work[36]. The lattice orientations of the HfO_2 variants for the two types of DWs are shown in the bottom panel of Figure 2C. In the left $O_{[010]}/O_{[001]}$ DW, as shown in the 3D model in Figure 2C, the polarization direction is vertically upward in $O_{[010]}$ forming 90° uncharged DW. In the right $O_{[001]}/O_{[010]}$ DW, as shown in the 3D model in Figure 2C, the polarization direction is horizontally to the right in $O_{[010]}$ 90° charged DW. The lattice constants of $Pca2_1$ HfO_2 unit cell are calculated to be a = 5.256 Å, b = 5.046 Å, and c = 5.073 Å, respectively, agreeing well with the previous measurements and calculations[19,36]. Based on the structural relaxation, it is seen that the thicknesses of the two types of DWs are as sharp as one unit cell (top panels of Figure 2D and E), which are in accordance with the experimental observation. These two DWs are proved to be the type (5) and type (10) DWs as defined in our previous work[36]. The energy densities of the two DWs are calculated to be 473.2 mJ/m^2 and 655.9 mJ/m^2, respectively. From the layer-resolved density of states (LDOS) of HfO_2 DWs shown in the bottom panels of Figure 2D and E, the left $O_{[010]}/O_{[001]}$ DW [Figure 2D] exhibits a flat band structure along the DW normal direction. In contrast, there is a band bending in the right $O_{[001]}/O_{[010]}$ DW structure [Figure 2E], which is caused by the charged DW. The ferroelectric polarization of one of the domain regions ($O_{[010]}$) is perpendicular to the right $O_{[001]}/O_{[010]}$ DW plane, leading to the positively charged (oxygen-ion diminishing) and negatively charged (oxygen-ion accumulating) interfaces and, hence, causes the energy band lifting and lowering at the two DWs, respectively.

Incoherent interface

After determining the positions of the two phases and their phase boundaries, we also investigated other structures present in this HZO film, as shown in Figure 3. The HZO thin film in Figure 3A appears to be divided into two halves from the middle, forming a split interface. To further study the characteristics of the two phases structure and the interface, we present enlarged images of the phase structure on the left and right sides of the interface in Figure 3B and D, respectively. Next, we analyze the lattice spacings of the two phases and the interface between them.

In Figure 3B, the lattice spacings perpendicular to each other for Hf atoms are measured to be 0.36 nm and 0.27 nm, respectively. In the phase shown in Figure 3D, the maximum lattice spacings but not vertical for Hf atoms are found to be 0.23 nm and 0.28 nm, respectively. By analyzing the FFT in Figure 3C and E of these phase structures and the arrangement of atoms, we get that the orientation of the crystal zone axis is

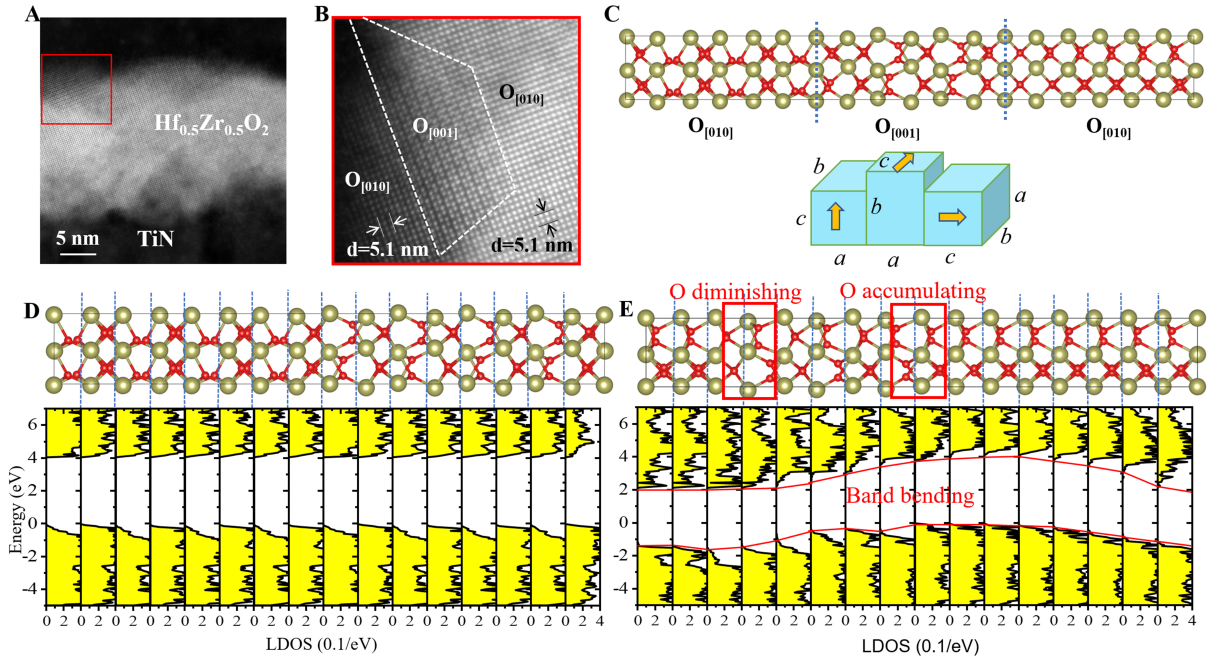

Figure 2. (A) HAADF-STEM image of HZO films with O phase; (B) An enlarged view of the red box in (A) indicates an HZO structure with two 90° domains; (C) The sketches of the two types of 90° DWs include left $O_{[010]}/O_{[001]}$ DW and right $O_{[001]}/O_{[010]}$ DW; (D-E) The atomic structures (top panels) and LDOS of two types of 90° DWs from the left and right DWs of Figure (C) respectively. Red rectangles mark the oxygen-ion diminishing and accumulating interfaces. Each layer of LDOS includes the states of two Hf and four O. HAADF-STEM: High-angle-annular-dark-field scanning transmission electron microscopy; HZO: $Hf_{0.5}Zr_{0.5}O_2$; DWs: domain walls; LDOS: layer-resolved density of states.

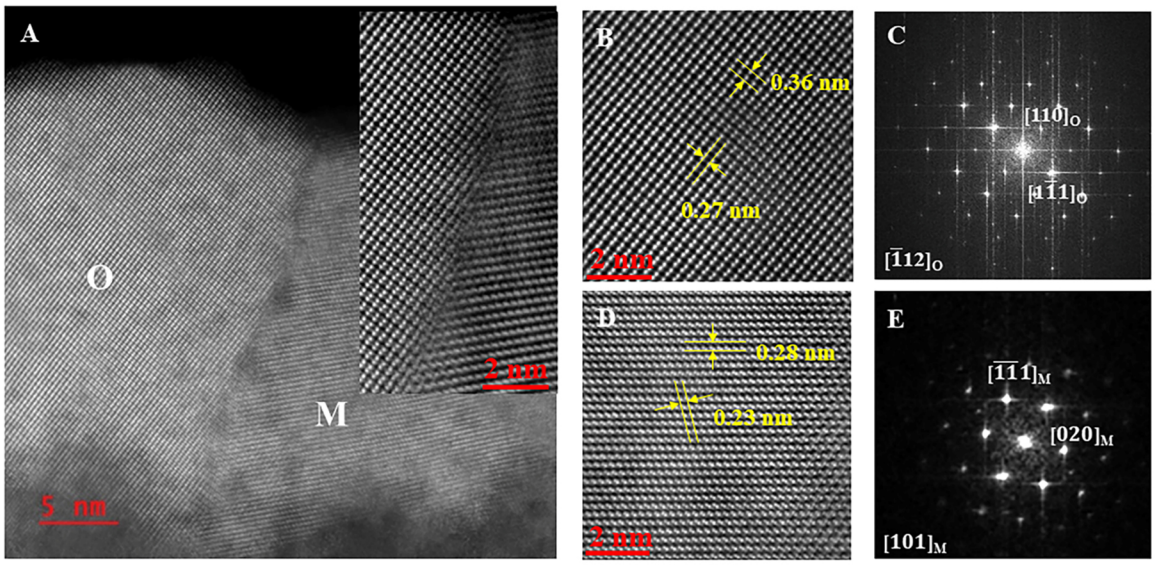

Figure 3. (A) Low magnification morphology image of grown TiN/HZO/TiN thin films, which have the incoherent interface; The inset is the high-magnification HAADF-STEM image of grown TiN/HZO/TiN thin films, which have the obvious stepped structure incoherent interface; (B) and (D) are enlarged images on the left and right sides of the interface in (A), respectively. (C) and (E) are FFT of (B) and (D), respectively. HZO: $Hf_{0.5}Zr_{0.5}O_2$; HAADF-STEM: high-angle-annular-dark-field scanning transmission electron microscopy; FFT: fast Fourier transform.

[$\bar{1}$12] in Figure 3B and the crystal zone axis is [101] in Figure 3D. Therefore, combining the axial orientation

of the phase structure, the lattice spacings, and the atomic arrangement, we conclude that this system represents a polyphase coexistence of the O phase and M phase. This indicates that the O phase and M phase are widely present in the film system, therefore demonstrating the feasibility and necessity of our study.

The inset of Figure 3A illustrates the interface between the O phase and M phase in this polyphase coexistence system. In comparison to the interface depicted in Figure 1B, this interface is classified as an incoherent interface. The distinguishing factor lies in the significant disparity between the lattice spacing of Hf atoms in the two phases, suggesting the presence of lattice distortion and twisting at the boundary between the two phases. Consequently, the mismatch at this interface is substantial, resulting in a high level of mismatch stress that gives rise to the incoherent phenomenon observed. According to the above analysis, it can be inferred that the interface represents a high-index interface, and displays an interface structure akin to a step-like configuration.

Comparison of the above interfaces: Firstly, in Figure 1B, we speculate that the presence of a transition layer in the coherent interface is due to the fact that the O phase possesses a non-centrosymmetric structure with polarization, whereas the M phase has a centrosymmetric structure without polarization. To alleviate the appearance of a polar and non-polar interface, a coherent lattice transition layer is formed. Additionally, the existence of the transition layer in the interface serves to alleviate strain mismatch. Although the lattice constants of the two phases are close, there is still an interface energy associated with the coherent interface. On the other hand, in the incoherent interface depicted in Figure 3A, the mismatch is significant under high index orientation, and the interface energy is generally greater than the coherent interface. Consequently, a stepped interface structure is formed to alleviate this mismatch. The appearance of low index and high index phases in the growth direction is due to the formation of columnar crystals in the bottom electrode, which results from the magnetron sputtering growth.

CONCLUSIONS

Based on the aforementioned analysis, the following conclusions can be drawn: Structure analysis of the HZO thin films reveals the presence of the two phase boundaries. One of these interfaces is the coherent interface with a low index orientation, which does not exhibit prominent interface characteristics. The different phase structures on both sides of this interface are verified through strain analysis and micro-region FFT analysis. The O phase/M phase boundary is observed to have a transition layer, and some boundaries appear to be non-straight due to the accumulation of oxygen vacancy caused by the presence of polarization charge. Next, we analyze the interface structure with two types of 90° domain structures. Through DFT simulation, we find that compared to the left $O_{[010]}/O_{[001]}$ 90° domain, band bending occurred in the 90° region of right $O_{[001]}/O_{[010]}$ DW. In the left $O_{[010]}/O_{[001]}$ DW, there has no band curvature because there is no depletion or accumulation of oxygen at the DW. However, the right $O_{[010]}/O_{[001]}$ DW will cause depletion and accumulation of O at the DW respectively as the polarization points towards or away from the domain wall. In the end, the other O phase/M phase boundary is composed of the two phase structures with high index lattice planes. Since this interface cannot achieve a coherent state, a stepped phase boundary structure is formed. This split interface structure may be the reason for the formation of polycrystals in HfO_2-based ferroelectric thin films. The findings of this study provide guidance for the analysis of phase structures and interface structures in HfO_2.

DECLARATIONS

Authors' contributions

The conception and design of the study: Zhang, S.; Liao, M.; Yang, Q.

The acquisition and analysis of data: Zhang, S.; Mu, X.; Wang, B.
The writing and revising: Zhang, S.; Liao, M.; Yang, Q.J.; Liao, J.; Zhou, Y.

Availability of data and materials

The raw data supporting the conclusions of this article will be made available by the corresponding author upon reasonable request.

Financial support and sponsorship

This work was partially supported by the Scientific Research Innovation Capability Support Project for Young Faculty (Grant No. ZYGXQNJSKYCXNLZCXM-M22), the National Key Research and Development Program of China (Grant No. 2024YFA1208603), the National Natural Science Foundation of China (Grant Nos. 52122205 and 51901166), the Natural Science Basic Research Program of Shaanxi (Grant No. 2024JC-YBQN-0583), and the Guangdong Basic and Applied Basic Research Foundation (No. 2022A1515110116).

Conflicts of interest

All authors declared that there are no conflicts of interest.

Ethical approval and consent to participate

Not applicable.

Consent for publication

Not applicable.

REFERENCES

1. Tang, Y. L.; Zhu, Y. L.; Ma, X. L.; et al. Ferroelectrics. Observation of a periodic array of flux-closure quadrants in strained ferroelectric $PbTiO_3$ films. *Science* **2015**, *348*, 547-51. DOI PubMed
2. Nelson, C. T.; Gao, P.; Jokisaari, J. R.; et al. Domain dynamics during ferroelectric switching. *Science* **2011**, *334*, 968-71. DOI PubMed
3. Wang, L.; Qi, H.; Deng, S.; et al. Design of superior electrostriction in $BaTiO_3$-based lead-free relaxors via the formation of polarization nanoclusters. *InfoMat* **2023**, *5*, e12362. DOI
4. Dawber, M.; Rabe, K. M.; Scott, J. F. Physics of thin-film ferroelectric oxides. *Rev. Mod. Phys.* **2005**, *77*, 1083-130. DOI
5. Scott, J. F. Applications of modern ferroelectrics. *Science* **2007**, *315*, 954-9. DOI PubMed
6. Wu, L.; Ji, Y.; Dan, H.; Bowen, C. R.; Yang, Y. A multifunctional optical-thermal logic gate sensor array based on ferroelectric $BiFeO_3$ thin films. *InfoMat* **2023**, *5*, e12414. DOI
7. Chisholm, M. F.; Luo, W.; Oxley, M. P.; Pantelides, S. T.; Lee, H. N. Atomic-scale compensation phenomena at polar interfaces. *Phys. Rev. Lett.* **2010**, *105*, 197602. DOI PubMed
8. Zhang, S.; Zhu, Y.; Tang, Y.; et al. Giant polarization sustainability in ultrathin ferroelectric films stabilized by charge transfer. *Adv. Mater.* **2017**, *29*, 1703543. DOI PubMed
9. Böscke, T. S.; Müller, J.; Bräuhaus, D.; Schröder, U.; Böttger, U. Ferroelectricity in hafnium oxide thin films. *Appl. Phys. Lett.* **2011**, *99*, 102903. DOI
10. Cheema, S. S.; Kwon, D.; Shanker, N.; et al. Enhanced ferroelectricity in ultrathin films grown directly on silicon. *Nature* **2020**, *580*, 478-82. DOI PubMed
11. Lee, H. J.; Lee, M.; Lee, K.; et al. Scale-free ferroelectricity induced by flat phonon bands in HfO_2. *Science* **2020**, *369*, 1343-7. DOI PubMed
12. Kim, S. B.; Ahn, Y. H.; Park, J.; Lee, S. W. Enhanced nucleation and growth of HfO_2 thin films grown by atomic layer deposition on graphene. *J. Alloys. Compd.* **2018**, *742*, 676-82. DOI
13. Chen, W.; Han, Q.; He, J.; He, W.; Wang, W.; Guo, H. Effect of HfO_2 framework on steam oxidation behavior of HfO_2 doped Si coating at high temperatures. *Ceram. Int.* **2022**, *48*, 20201-10. DOI
14. Peng, Y.; Wang, Z.; Xiao, W.; et al. Effect of thickness scaling on the switching dynamics of ferroelectric HfO_2-ZrO_2 capacitors.

Ceram. Int. **2022**, *48*, 28489-95. DOI
15. Luo, Q.; Cheng, Y.; Yang, J.; et al. A highly CMOS compatible hafnia-based ferroelectric diode. *Nat. Commun.* **2020**, *11*, 1391. DOI PubMed PMC
16. Müller, J.; Böscke, T. S.; Schröder, U.; et al. Ferroelectricity in simple binary ZrO_2 and HfO_2. *Nano. Lett.* **2012**, *12*, 4318-23. DOI PubMed
17. Batra, R.; Huan, T. D.; Jones, J. L.; Rossetti, G.; Ramprasad, R. Factors favoring ferroelectricity in hafnia: a first-principles computational study. *J. Phys. Chem. C.* **2017**, *121*, 4139-45. DOI
18. Xu, X.; Huang, F. T.; Qi, Y.; et al. Kinetically stabilized ferroelectricity in bulk single-crystalline HfO_2:Y. *Nat. Mater.* **2021**, *20*, 826-32. DOI PubMed
19. Sang, X.; Grimley, E. D.; Schenk, T.; Schroeder, U.; Lebeau, J. M. On the structural origins of ferroelectricity in HfO_2 thin films. *Appl. Phys. Lett.* **2015**, *106*, 162905. DOI
20. Lebeau, J. M.; D'alfonso, A. J.; Wright, N. J.; Allen, L. J.; Stemmer, S. Determining ferroelectric polarity at the nanoscale. *Appl. Phys. Lett.* **2011**, *98*, 052904. DOI
21. Schroeder, U.; Yurchuk, E.; Müller, J.; et al. Impact of different dopants on the switching properties of ferroelectric hafniumoxide. *Jpn. J. Appl. Phys.* **2014**, *53*, 08LE02. DOI
22. Schroeder, U.; Materano, M.; Mittmann, T.; Lomenzo, P. D.; Mikolajick, T.; Toriumi, A. Recent progress for obtaining the ferroelectric phase in hafnium oxide based films: impact of oxygen and zirconium. *Jpn. J. Appl. Phys.* **2019**, *58*, SL0801. DOI
23. Kim, H. J.; Park, M. H.; Kim, Y. J.; et al. Grain size engineering for ferroelectric $Hf_{0.5}Zr_{0.5}O_2$ films by an insertion of Al_2O_3 interlayer. *Appl. Phys. Lett.* **2014**, *105*, 192903. DOI
24. Lee, A. J.; Kim, B. S.; Hwang, J. H.; et al. Controlling the crystallinity of HfO_2 thin film using the surface energy-driven phase stabilization and template effect. *Appl. Surf. Sci.* **2022**, *590*, 153082. DOI
25. Shimizu, T.; Mimura, T.; Kiguchi, T.; et al. Ferroelectricity mediated by ferroelastic domain switching in HfO_2-based epitaxial thin films. *Appl. Phys. Lett.* **2018**, *113*, 212901. DOI
26. Zheng, Y.; Xin, T.; Yang, J.; et al. *In-situ* atomic-level observation of reversible first-order transition in $Hf_{0.5}Zr_{0.5}O_2$ ferroelectric film. In: 2022 International Electron Devices Meeting (IEDM); 2022 Dec 3-7; San Francisco, CA, USA. New York: IEEE; **2022**. pp 6.3.1-6. 3.4. DOI
27. Zheng, Y.; Zhang, Y.; Xin, T.; et al. Direct atomic-scale visualization of the 90° domain walls and their migrations in $Hf_{0.5}Zr_{0.5}O_2$ ferroelectric thin films. *Mater. Today. Nano.* **2023**, *24*, 100406. DOI
28. Fina, I.; Sánchez, F. Seeing ferroelectric phase transitions. *Nat. Mater.* **2024**, *23*, 1015-6. DOI PubMed
29. Li, X.; Liu, Z.; Gao, A.; et al. Ferroelastically protected reversible orthorhombic to monoclinic-like phase transition in ZrO_2 nanocrystals. *Nat. Mater.* **2024**, *23*, 1077-84. DOI PubMed
30. Pešić, M.; Fengler, F. P. G.; Larcher, L.; et al. Physical mechanisms behind the field-cycling behavior of HfO_2-based ferroelectric capacitors. *Adv. Funct. Materials.* **2016**, *26*, 4601-12. DOI
31. Kim, H. J.; Park, M. H.; Kim, Y. J.; et al. A study on the wake-up effect of ferroelectric $Hf_{0.5}Zr_{0.5}O_2$ films by pulse-switching measurement. *Nanoscale* **2016**, *8*, 1383-9. DOI PubMed
32. Cheng, Y.; Gao, Z.; Ye, K. H.; et al. Reversible transition between the polar and antipolar phases and its implications for wake-up and fatigue in HfO_2-based ferroelectric thin film. *Nat. Commun.* **2022**, *13*, 645. DOI PubMed PMC
33. Grimley, E. D.; Schenk, T.; Mikolajick, T.; Schroeder, U.; Lebeau, J. M. Atomic structure of domain and interphase boundaries in ferroelectric HfO_2. *Adv. Materials. Inter.* **2018**, *5*, 1701258. DOI
34. Shi, S.; Xi, H.; Cao, T.; et al. Interface-engineered ferroelectricity of epitaxial $Hf_{0.5}Zr_{0.5}O_2$ thin films. *Nat. Commun.* **2023**, *14*, 1780. DOI PubMed PMC
35. Zhang, S.; Zhu, M.; Suriyaprakash, J.; et al. Flux-closure domains in $PbTiO_3$/$SrTiO_3$ multilayers mediated without tensile strain. *J. Phys. Chem. C.* **2022**, *126*, 4630-7. DOI
36. Ding, W.; Zhang, Y.; Tao, L.; Yang, Q.; Zhou, Y. The atomic-scale domain wall structure and motion in HfO_2-based ferroelectrics: a first-principle study. *Acta. Mater.* **2020**, *196*, 556-64. DOI